BIOLOGY Methods & Protocols

Biology Methods and Protocols, 2022, 1–12

https://doi.org/10.1093/biomethods/bpac003
Advance Access Publication Date: 12 January 2022
Methods Article

METHODS ARTICLE

Improving one-step scarless genome editing in *Drosophila melanogaster* by combining *ovo*^{D} co-CRISPR selection with sgRNA target site masking

Katharina J. Götze[1,†], Achmed Mrestani [1,2,3,†], Paula Beckmann[1], Knut Krohn[4], Diana Le Duc [5], Akhil Velluva[5,6], Mathias A. Böhme[1], Manfred Heckmann[2], Rami Abou Jamra[5], Johannes R. Lemke [5], Hendrik Bläker[7], Nicole Scholz [1], Dmitrij Ljaschenko[1,*] and Tobias Langenhan [1,*]

[1]Rudolf Schönheimer Institute of Biochemistry, Division of General Biochemistry, Medical Faculty, Leipzig University, Leipzig 04103, Germany, [2]Institute of Physiology, Department of Neurophysiology, University of Würzburg, Würzburg 97070, Germany, [3]Department of Neurology, University of Leipzig Medical Center, Leipzig 04103, Germany, [4]Core Unit DNA, Medical Faculty, University of Leipzig Medical Center, Leipzig 04103, Germany, [5]Institute of Human Genetics, University of Leipzig Medical Center, Leipzig 04103, Germany, [6]Department of Evolutionary Genetics, Max Planck Institute for Evolutionary Anthropology, Leipzig 04103, Germany and [7]Institute of Pathology, University of Leipzig Medical Center, Leipzig 04103, Germany

[†]These authors contributed equally to this work
*Correspondence address. (D.L.) Rudolf Schönheimer Institute of Biochemistry, Division of General Biochemistry, Medical Faculty, Leipzig University, Johannisallee 30, Leipzig 04103, Germany. Tel: +49 341 9722105; +49 (341) 97-22109; E-mail: Dmitrij.Ljaschenko@medizin.uni-leipzig.de. (T.L.) Rudolf Schönheimer Institute of Biochemistry, Division of General Biochemistry, Medical Faculty, Leipzig University, Johannisallee 30, Leipzig 04103, Germany. Tel: +49 341 9722100; +49 (341) 97-22109; E-mail: tobias.langenhan@gmail.com

Abstract

The precise and rapid construction of alleles through CRISPR/Cas9-mediated genome engineering renders *Drosophila melanogaster* a powerful animal system for molecular structure–function analyses and human disease models. Application of the *ovo*^{D} co-selection method offers expedited generation and enrichment of scarlessly edited alleles without the need for linked transformation markers, which specifically in the case of exon editing can impact allele usability. However, we found that knockin procedures by homology-directed repair (HDR) under *ovo*^{D} co-selection resulted in low transformation efficiency. This is likely due to repeated rounds of Cas9 cleavage of HDR donor and/or engineered genomic locus DNA, as noted for other CRISPR/Cas9 editing strategies before, impeding the recovery of correctly edited alleles. Here we provide a one-step protocol to improve the generation of scarless alleles by *ovo*^{D}-co-selection with single-guide RNA (sgRNA) binding site masking. Using this workflow, we constructed human disease alleles for two *Drosophila* genes, *unc-13/CG2999* and *armadillo/CG11579*. We show and quantify how a known countermeasure, the insertion of silent point mutations into protospacer

Received: 28 October 2021; **Revised:** 28 December 2021; **Editorial Decision:** 7 January 2022; **Accepted:** 10 January 2022

adjacent motif (PAM) or sgRNA homology regions, can potently suppress unintended sequence modifications during CRISPR/Cas9 genome editing of *D. melanogaster* under ovo^D co-selection. This strongly increased the recovery frequency of disease alleles.

Keywords: CRISPR; Cas9; genome engineering; Munc13; armadillo; neurodevelopmental disorder; synapse; cancer; *Drosophila*

Introduction

Based on the concerted human genome sequencing efforts of the past two decades, scientists and clinicians have access to detailed genetic information associated with a plethora of human diseases [1–3]. In model organisms with a suitably homologous gene set and amenability to gene targeting technologies, this information can ultimately be used to test for causality between mutation and disease state [4]. Such an approach provides a solid basis for defining the pathophysiological underpinnings of a human ailment and its genetic characteristics. The fashioning of RNA-guided Cas9 endonuclease activity selected positions in genomic DNA, now commonly referred to as CRISPR/Cas9 genome engineering, has expedited the generation of human disease models. The CRISPR/Cas9 methodology allows for precise and rapid genome editing in human cells [5–7] and a large array of model species including the fruit fly *Drosophila melanogaster* [8–12], which is successfully used as a model for human diseases [13–16].

Direct scarless insertion of human mutations into the *Drosophila* genome via CRISPR/Cas9-assisted homology-directed repair (HDR) affords the separation of the targeting template part, which carries the engineered disease mutation, from the selection marker required for transformant identification. A recently introduced method that utilizes a negative transformant selection strategy rests on co-editing of a female sterile ovo^{D1} allele and offers an elegant solution for this technical complication [17]. Using ovo^D co-selection, the successful editing event at the target locus is identified by simultaneous correction of the ovo^{D1}-inflicted sterility, thereby enriching for CRISPR/Cas9 events. However, when we applied ovo^D co-selection for the generation of candidate, human pathogenic allele sets for two independent genes, *unc-13* (human homolog: *Munc13-3*) and *armadillo* (human homolog: *CTNNB1*), by an HDR approach, we noticed unacceptably low targeting success rates. Inadvertent sequence errors were introduced at the genomic Cas9 cleavage sites during the targeting procedure likely through repeated Cas9 cleavage of the engineered locus. This was caused by incorporation of single-guide RNA (sgRNA) binding site sequences that were identical to the original gene sequence in the HDR plasmid. Due to the same reason, we found no transformants at all in another independent targeting experiment. Here, Cas9 processing of the HDR plasmid DNA effectively separated the repair sequence from its flanking homology arms and thus impeded gene targeting.

Results from CRISPR/Cas9 engineering in *Saccharomyces cerevisiae* have offered approaches to circumvent these problems either by the introduction of silent mutations in protospacer adjacent motif (PAM) sites [18] or by the insertion of blocks of sequence heterology into the sgRNA motif [19]. While these procedures were suggested to be fundamentally applicable to *Drosophila* genome engineering as well [9, 20, 21] and were successfully applied with single-stranded oligodeoxynucleotides as the donor template [22], quantitative assessment of such protective strategies for well-established CRISPR/Cas9 protocols using double-stranded donor templates [9, 10] in combination with ovo^D co-selection is lacking. Here we provide such analysis and highlight guidelines for HDR plasmid construction to prevent undesired repeated target sequence cleavage. We show that this strategy ensures high success rates with enrichment of CRISPR/Cas9 editing events by ovo^D co-selection, for example, in the construction of human disease models. Nonetheless, these findings are likely of general interest for CRISPR/Cas9 editing experiments and not limited to ovo^D-co-CRISPR approaches.

Materials and methods

Molecular reagents

All primer sequences used in this study are listed in Supplementary Table S1.

pU6-sgRNAs

CRISPR/Cas9 cutting sites 5′ and 3′ of the *unc-13* and *arm* loci were identified by "CRISPR Optimal Target Finder" [10]. The genomic sequences of all CRISPR/Cas9 cleavage sites were confirmed by DNA sequencing of PCR fragments encompassing the suggested sites prior to cloning. Target-specific sequences for *unc-13* sgRNAs were synthesized as 5′-phosphorylated oligonucleotides, annealed, and ligated into the *BbsI* sites of the *pU6-BbsI-chiRNA* vector [9], sgRNAs for *arm* targeting plasmids were synthesized by GenScript Biotech B.V. (The Netherlands) (Supplementary Table S2).

unc-13 HDR vectors

To generate mutation cluster 1 HDR vectors, a 4.3-kb product was PCR-amplified from w^{1118} genomic DNA using primers am_226F/am_223R and, after gel purification, was *Sac*II/*Avr*II cut and ligated into a 2.8-kb backbone fragment of *Sac*II/*Avr*II-digested *pHD-DsRed-attP* (pTL620), which gave rise to pAM66. For mutation cluster 2 HDR vectors, a 3.9-kb product was PCR-amplified from w^{1118} genomic DNA using primers am_227f and am_225r and, after gel purification, was *Sac*II/*Avr*II cut and ligated in a 2.8-kb backbone fragment of SacII/AvrII-digested *pHD-DsRed-attP* (pTL620), which gave rise to pAM67. Quikchange mutagenesis to introduce the respective nucleotide exchanges was performed using Pfu DNA polymerase (Promega) in combination with *DpnI* digest to clear original bacterial plasmid background using primers optimized for *Drosophila* codon usage, carrying the mutated nucleotides contained by 12- to 21-bp flanking homologous sequences. Details are listed in Supplementary Table S3.

arm HDR vectors

To generate the *arm* HDR vector kit, a 1.5 kb fragment of w^{1118} genomic sequence was synthesized and cloned into *pHD-DsRed-attP* (pTL620) generating pTL947. All further mutations and modifications to the *arm* fragment were introduced into this plasmid as outlined in Supplementary Table S3.

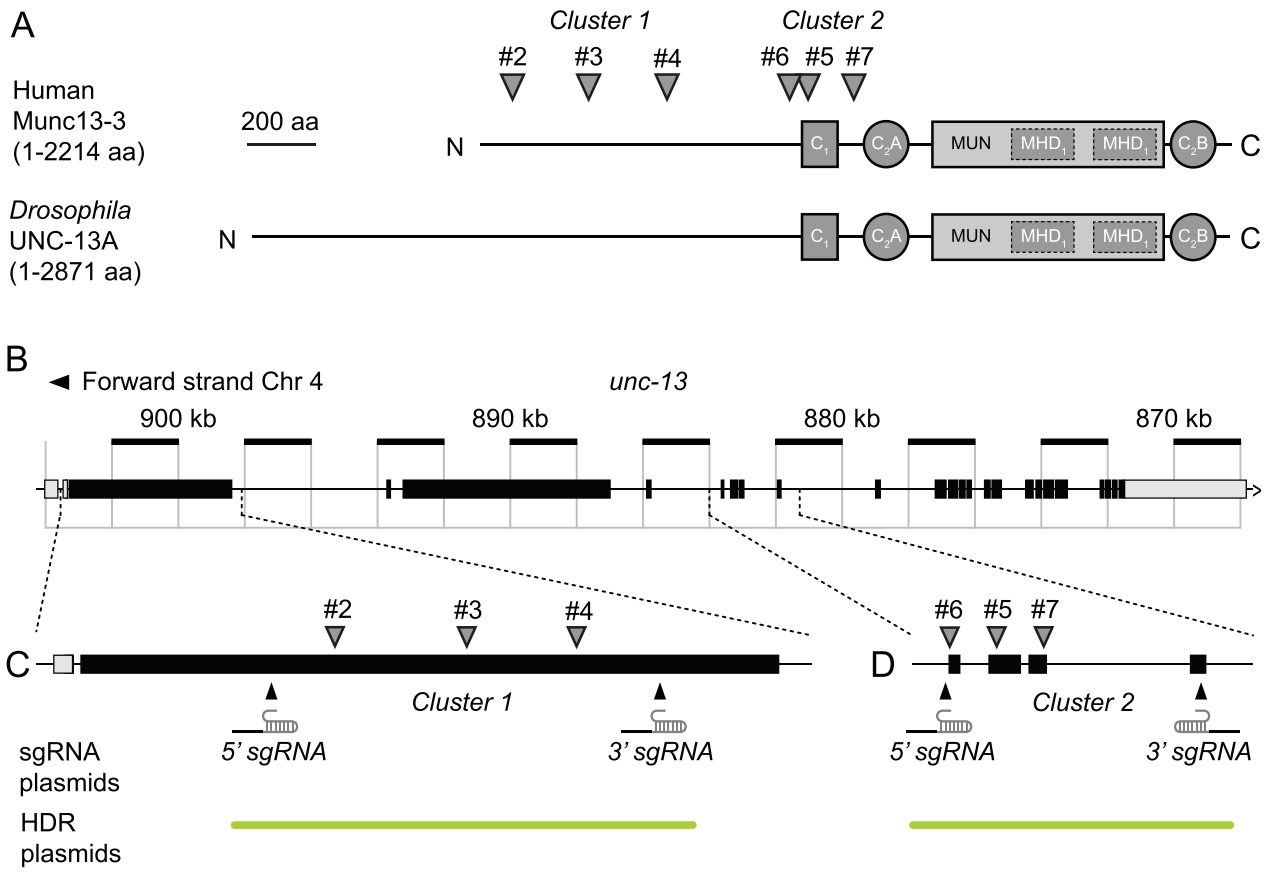

E

Site #	sgRNA sequence (5'-3') Distal	Proximal	PAM	Strand	OFF target #
Cluster 1					
5' sgRNA	GCTGATCC	GGGCCCGCTATA	TGG	–	0
HDR-fixed	**GCTGATCC**	**tGGaCCcgagTA**	**gGG**		
3' sgRNA	TCATCATC	ATATACCTCCGT	CGG	–	1 (X)
	TaATtAaa	ATATAtCTCCGT	CGG		
HDR-fixed	**TCATCATC**	**gTAcACtTCtGT**	**gGG**		
Cluster 2					
5' sgRNA	TTGTCTAA	AGGGACGTAACG	AGG	–	1 (3L)
	TTGcacAA	AGGGACGaAACG	AGG		
3' sgRNA	CAGTTGAG	GGAACATCTAAG	TGG	+	0

Figure 1: *ovo*^{D}-assisted CRISPR/Cas9 editing of *unc-13* with masked proximal sgRNA binding sites. (**A**) Schematic of the domain structure of the human Munc13-3 and the *Drosophila* UNC-13 proteins. The human disease-associated mutations are organized into two clusters. Relative locations of the mutations in the proteins are indicated by downward triangles. (**B**) Schematic of the *Drosophila unc-13* locus. Black boxes indicate exons, and light gray boxes indicate UTRs. (**C** and **D**) Enlarged view of the regions harboring the sgRNA binding site pairs used for Cas9 targeting to generate cluster 1 (C) and cluster 2 (D) mutations. Downward triangles mark the positions of the point mutations. (**E**) sgRNA sequences for cluster 1 (upper box) and cluster 2 (lower box) targeting. Off-target binding sites as predicted by *FlyCRISPR optimal target finder* are indicated in gray below the respective sgRNA binding site. Modified nucleotides used to mask sgRNA binding sites in the HDR plasmid for improved *ovo*^{D}-assisted CRISPR/Cas9 targeting of cluster 1 are marked by lowercase letters in red. Note that the PAM sites of both modified sgRNA sites for cluster 1 maintain a NGG sequence and are thus, on their own, not suitable for Cas9 cleavage suppression. Cas9 cleavage site is indicated by blue triangles. Strand direction relative to genomic *unc-13* sequence (+, forward strand; –, reverse strand).

sgRNA binding site modifications in HDR-fixed vectors

To prevent Cas9 cleavage of HDR vectors, silent mutations were introduced into sgRNA binding and PAM sites for *unc-13* cluster 1: 6 nucleotides (nt) of the 5′-sgRNA binding site + 1 nt of its PAM site, and 4 nt of the 3′-sgRNA site + 1 nt of its PAM site were exchanged, respectively (Fig. 1E). For *arm* modifications, the 5′- and 3′-PAM sites were mutated by two and a single silent mutation (Fig. 4C), respectively. Modifications were performed at GenScript (Supplementary Table S3).

Genotyping of mutant fly strains

Genotyping was performed via Sanger sequencing. Primer pairs for each mutation and each sgRNA binding site, respectively, were designed (*unc-13*$^{\#2}$: am_255F/am_256R; *unc-13*$^{\#3}$: am_245F/am_257R; *unc-13*$^{\#4}$: am_258F/am_259R; *unc-13*$^{\#5}$: am_242F/am_252R; *unc-13*$^{\#6}$: am_253F/am_219R; *unc-13*$^{\#7}$: am_254F/am_252R; cluster 1 – 5′-sgRNA binding site: kg_14F/kg_15R; cluster 1 – 3′-sgRNA binding site: kg_16F/kg_17R; cluster 2 – 5′-sgRNA binding site: kg_18F/kg_19R; cluster 2 – 3′-sgRNA binding site: kg_20F/kg_21R; *arm:* tl_911F/tl_914R).

Mutation	Genotype	Lines	Stock ID
unc-13$^{\#2}$	*unc-13*$^{V675F(pAM75)}$/*In(4)ci*^{D}	1–3	DL0101–DL0103
unc-13$^{\#3}$	*unc-13*$^{D923E(pAM76)}$/*In(4)ci*^{D}	1–3	DL0104 –DL106
unc-13$^{\#4}$	*unc-13*$^{D1136C(pAM77)}$/*In(4)ci*^{D}	1–3	DL0107–DL109
unc-13$^{\#5}$	*unc-13*$^{T1729M(pAM68)}$/*In(4)ci*^{D}	1	DL0092
		2	DL0091
		3	DL0090
		4–8	DL0114–DL0118
unc-13$^{\#6}$	*unc-13*$^{A1679I(pAM69)}$/*In(4)ci*^{D}	1	DL0095
		3	DL0097
		4–5	DL0110–DL0111
unc-13$^{\#7}$	*unc-13*$^{I1814T(pAM70)}$/*In(4)ci*^{D}	1	DL0098
		3	DL0100
		4–5	DL0112–DL0113
unc-13$^{\#2\text{-}mod}$	*unc-13*$^{\#2\text{-}mod}$/*In(4)ci*^{D}	1–10	Not applicable
unc-13$^{\#3\text{-}mod}$	*unc-13*$^{\#3\text{-}mod}$/*In(4)ci*^{D}	1–10	Not applicable
arm^{WT}	*arm*^{WT}/*P{Tb1}FM7a, B sc v w y*	1–3	Not applicable
arm$^{\#2}$	*arm*$^{\#2}$/*P{Tb1}FM7a, B sc v w y*	1–12	Not applicable

Fly strains

Generated in this work

AA numbering refers to *D. melanogaster* UNC-13A isoform (Uniprot ID: Q8IM87).

CRISPR/Cas9 targeting

BDSC #56552, *w*^{1118}; *PBac{y*$^{+mDint2}$*=vas-Cas9}*^{VK00037}*/CyO, P{w*$^{+mC}$*=Tb*^{1}*}Cpr*$^{CyO\text{-}A}$*;;*

BDSC #55821, y^{1} *M{vas-Cas9.RFP*$^{-}$*}ZH-2A w*^{1118}*;;;* (both a gift by Kate O'Connor-Giles and Jill Wildonger, University of Wisconsin, Madison, WI, USA)

BDSC #1309, *ovo*^{D1} *v*^{24}*/C(1)DX,* y^{1} *w*^{1} *f*^{1}*;;;*

BDSC #78782, y^{1} *sc** *v*^{1} *sev*^{21}*;; P{y*$^{+t7.7}$ *v*$^{+t1.8}$*=nos-Cas9.R}*^{attP2}.

Other strains

BDSC #4759, *w*^{1118}*; P{w*$^{+mC}$*=ActGFP}unc-13*^{GJ}*/pan*^{2}

BDSC #24488, y^{1} *M{RFP[3xP3.PB] GFP[E.3xP3]=vas-int.Dm}*$^{ZH\text{-}2A}$ *w***; M{3xP3-RFP.attP}*$^{ZH\text{-}102D}$

DGRC #101911, *ry*^{506}*; P{ry[+t7.2]=ry11}unc-13*^{P84200}*/ci*^{D} *(= unc-13*^{KO} *allele)*

w^{1118} (Flybase ID: FBal0018186)

ovo^{D}*-assisted* CRISPR/Cas9 gene targeting

All transgenesis steps were performed at Bestgene Inc. (USA). To generate *unc-13* and *arm* mutant alleles, *ovo*^{D} Co-selection was performed as previously described [17]. Male flies harboring the dominant negative *ovo*^{D1} mutation on the X-chromosome (BDSC#1309) were crossed to nos-Cas9 expressing female virgins (BDSC #78782). Offspring embryos (F0) were injected with pAM63 (Addgene plasmid # 111142, pCFD3-ovo^{D1}-2 [17]) to target *ovo*^{D1}, a set of 5′- and 3′-sgRNA target plasmids and one HDR donor plasmid. F0 females were pooled and crossed to male flies expressing suitable chromosome balancers. F1 flies were then single-crossed to balancer flies, and clonal founder lines were identified by genotyping with suitable primers as indicated.

Sanger sequencing

Sequencing of defined fragments of DNA, for example, for investigation of possible genomic off-target events, sgRNA binding site errors, and mutation carriage was performed via Sanger sequencing at Microsynth AG (Switzerland). Genomic DNA was extracted with NucleoSpin Tissue kit (Machery-Nagel). With suitable primers, DNA fragments of interest less than 1000 bp were amplified via PCR. Gel electrophoresis was performed to separate the DNA bands. QIAEXII gel extraction kit (QIAGEN) was used to purify the DNA. In 1.5 ml tubes, the extracted DNA, water, and forward or reverse primer were mixed and sent to Microsynth AG or Eurofins. Sequencing results were analyzed with a plasmid editor.

Genome sequencing

Genomic DNA was extracted from adult fly homogenate samples using a NucleoSpin Tissue kit (Machery-Nagel). 40 ng of the DNA was used to prepare paired-end libraries with the Nextera DNA Library Prep kit (Illumina, San Diego, USA). The barcoded libraries were purified and quantified using Qubit Fluorometric Quantification (ThermoFischer Scientific). Size distribution of the library DNA was analyzed employing the FragmentAnalyzer (Agilent). Sequencing of 2×150 bp was performed with a NovaSeq sequencer (Illumina). Demultiplexing of raw reads, adapter trimming, and quality filtering were performed according to Stokowy *et al.* [23]. Resulting read pairs were mapped to the *Drosophila* r6 genome using the Burrows–Wheeler aligner [24] and visualized using the Integrative Genomics Viewer v2.9.4 [25]. Freebayes v.1.3.5 (https://arxiv.org/abs/1207.3907) was employed for variant calling and SnpEff v5.0e for variant annotation [26]. Only variants with an allele frequency of ≥20, sequencing depth of ≥30, and genotype quality of ≥20 were considered in our analysis. Furthermore, CNVkit was used for copy number variation identifications [27]. All changes were manually inspected and visualized.

unc-13 lethality assay

Lethality assays were performed by crossing 20 virgin female flies of *unc13*^{X}*/ci*^{D} stocks with 10 male *unc13ActGFP*^{KO}*/pan*^{2} flies (depicted in Fig. 2A as *unc13*^{KO}*/pan*^{2} for clarity reasons) at 25°C. The flies were transferred to a fresh vial every other day. Three vials per cross were used to determine the Mendelian ratios three

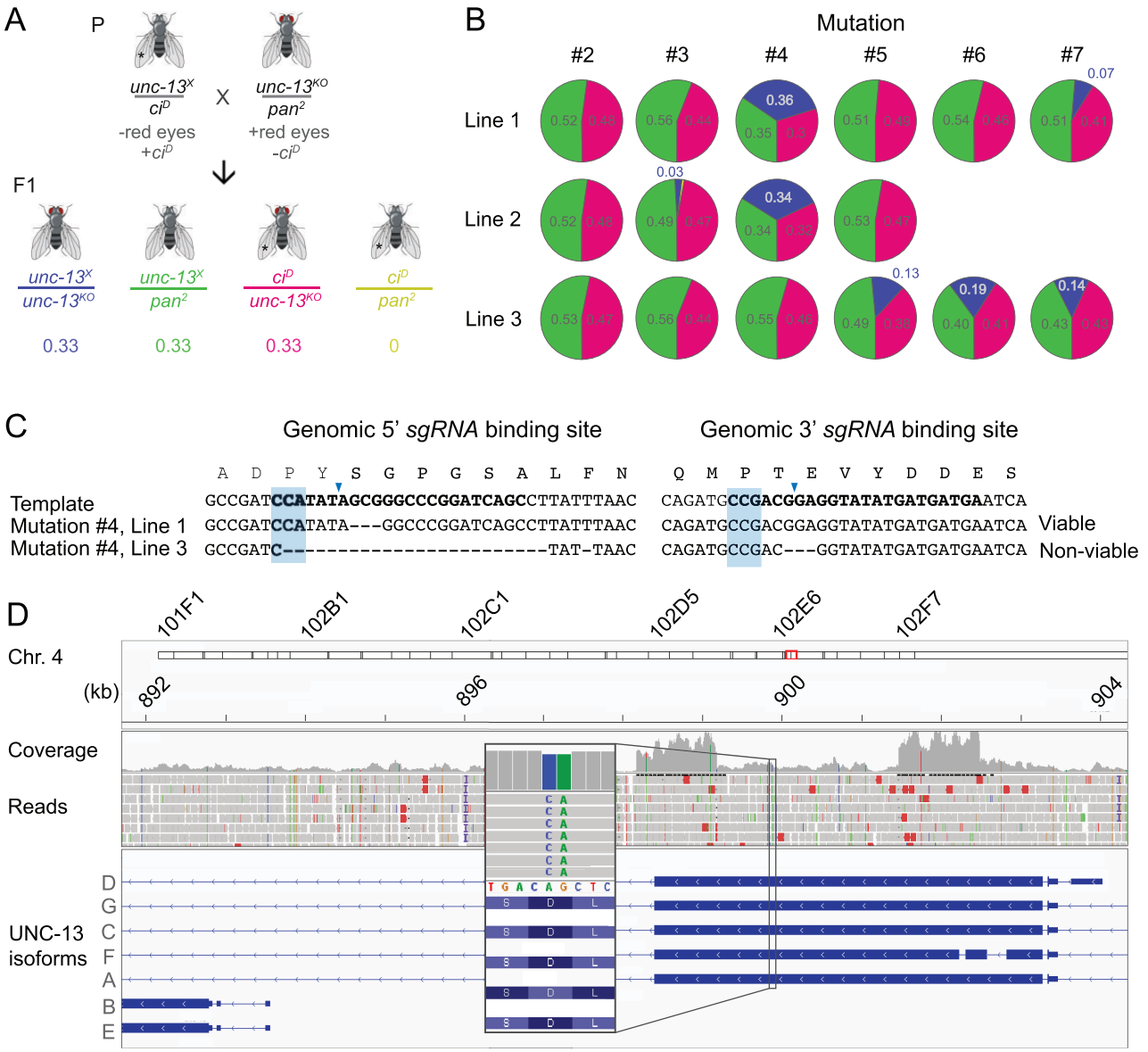

Figure 2: Repeated ovo^{D1}-assisted HDR gene targeting causes mutations at Cas9 cleavage sites and produce UNC-13 mutants with varying degrees of viability. (**A**) Crossing scheme for lethality assay of UNC-13 mutants. Expected genotype ratio of offspring shown at the bottom assuming that an *unc-13*^{x} mutation does not impede protein function. In one line, pan^2/ci^D escapers emerged (yellow pies: <0.1%). (**B**) Observed Mendelian ratios for *unc-13*^{x} mutations. For each mutation, two or three independently generated lines were tested. For mutations #3–#7, divergent viability levels are observed between different clonal stocks per mutation, indicating allelic differences between the clones. Blue = *unc-13*^{x}/*unc-13*^{KO}; green = *unc-13*^{x}/pan^2; magenta = ci^D/*unc-13*^{KO}; yellow = ci^D/pan^2. Total number of counted flies are: #2: 2284; #3: 2106; #4: 2706; #5: 3555; #6: 2717; #7: 2111. (**C**) Exemplary alignment of the 5′- and 3′-sgRNA binding site regions from *unc-13*$^{\#4}$ lines 1 and 3 obtained by Sanger sequencing of a PCR-amplified fragment covering the sites. The incorporation of inadvertent mutations of the locus leads to inconsistent results in viability assays, as the gene product contains different changes even within one targeting experiment. The blue boxes indicate PAM sites and the blue triangles the Cas9 cleavage position. (**D**) Indels at CRISPR sites as shown in (C) were confirmed using genome sequencing. Additionally, we looked for other undesired sequence changes. No additional changes, which could explain the lethality, were detected. Here the successful introduction of the UNC-13 mutation #4 in fly line 2 (inset) is depicted. For analysis, the Integrative Genomics Viewer was employed [25]. The red box indicates the position of the zoomed alignment on the target chromosome. *Coverage* indicates the relative number of reads for each position. The alignment of reads (forward strand) is shown below (gray = identical to the reference *Drosophila* r6 genome. Positions different to the reference are color coded: red = T; blue = C; green = A, orange = G). Red stretches in the alignment represent randomly distributed reads with selective low quality caused by sequencing errors. Blue "I"s represent insertions. The inset shows changed positions (C, A instead of T, C) in the alignment of reads (forward strand). Below the reverse strand DNA sequence and the corresponding amino acid sequence are shown.

times independently ($n = 9$). In all experiments, the results from the three independent crosses were very similar, which allowed pooling the results. Twenty days after the transferral to a new vial, the adult F1 generation was sorted and the number of individuals was counted based on their phenotype. The results were evaluated by calculating the mean fraction of each phenotype.

Results

Inadvertent sequence alterations at Cas9 cleavage sites during HDR genome editing with ovo^D co-selection

In order to study synaptic release in the context of neurodevelopmental disorders and active zone (AZ) dysfunction, we set

Table 1: Human *Munc13-3* and *CTNNB1* alleles

Allele description (shorthand)	Human mutation	Fly mutation
unc-13$^{\#2}$	C69F	V675F
unc-13$^{\#3}$	A319E	D923E
unc-13$^{\#4}$	R548C	D1136C
unc-13$^{\#5}$	T1104M	T1729M
unc-13$^{\#6}$	T1053I	A1679I
unc-13$^{\#7}$	I1189T	I1814T
arm$^{\#1}$	delW25-I35	delW35-I46
arm$^{\#2}$	S37C	S48C
arm$^{\#3}$	T41A	T52A
arm$^{\#4}$	S45F	S56F

Amino acid numbering to human and fly homologs. Reference protein sequences: MUNC13-3 (#Q8NB66), UNC-13A (#Q8IM87), CTNNB1 (#P35222), and ARM (#P18824).

out to construct *Drosophila* alleles containing human missense mutations of the AZ component Munc13-3/UNC-13. Munc13 homologs are multi-domain proteins (Fig. 1A) and exert evolutionarily highly conserved steps in synaptic vesicle priming [28–30]. In addition, Munc13 proteins govern the nano-architecture of AZs by positioning synaptic vesicles at defined coupling distances to the release triggering calcium channel complex [31].

To generate point mutated *unc-13* alleles, we first determined the position of the amino acid exchanges by aligning the human *Munc13-3* gene product, in which the mutations were originally identified, and isoforms of the *Munc13-3* homolog UNC-13 of *D. melanogaster*. The location of three of these human missense mutations (#2, #3, #4; cluster 1) was mapped to an N-terminal region of the UNC-13A isoform, which shows low structural complexity without known protein domains (Fig. 1A). Cluster 1 mutations are located close to each other in a large exon spanning 4890 bp (Fig. 1B and C), which is exclusively spliced into mRNA species encoding the fly UNC-13A isoform [31]. The remaining three mutations (#5, #6, #7; cluster 2) are based in the C-terminal area of UNC-13 with one of them affecting the diacylglycerol/phorbol ester binding C1 domain (Fig. 1A) [32]. This cluster of small exons is present in both major UNC-13 isoforms A and B of *Drosophila* (cluster 2; Fig. 1B and D; Table 1).

In order to allow editing within the target exons and to expedite allele construction, we employed a recently introduced CRISPR/Cas9-assisted genomic engineering workflow utilizing a co-edited X-linked hypomorphic *ovo*^{D1} allele. Female carriers of the dominant *ovo*^{D1} hypomorphic allele display penetrant sterility due to defective oocyte development. As genomic editing of the *ovo*^{D1} allele can restore female fertility, successful co-editing of nonlinked target genes can be enriched for by a simple negative selection strategy [17].

We identified two pairs of suitable sgRNA binding sites flanking the target exon clusters 1 and 2, respectively, in which the missense mutations needed to be placed (Fig. 1A). Then, we generated an HDR plasmid for each exon cluster, which contained the respective part of the *unc-13* genomic locus to be removed through the CRISPR/Cas9 intervention. In addition, both HDR plasmids provided large homology arms extending more than 1 kb distance beyond the location of the human mutations to be inserted and included the native sgRNA binding sequences (Fig. 1E). Each *Munc13-3* missense mutation was then individually introduced into the respective HDR vector to generate two sets of plasmids (cluster 1: *pHDR-unc-13*$^{\#2}$, *pHDR-unc-13*$^{\#3}$, *pHDR-unc-13*$^{\#4}$; cluster 2: *pHDR-unc-13*$^{\#5}$, *pHDR-unc-13*$^{\#6}$, *pHDR-unc-13*$^{\#7}$) for transgenesis. Next, for the two sgRNA plasmids to release the *unc-13* target exon cluster, the respective HDR plasmid for DNA double-strand break (DSB) repair with the mutated genome fragment, and a single sgRNA for *ovo*^{D} editing were co-injected into *ovo*^{D1} embryos with constitutive germline expression of Cas9 from a *nos-Cas9* transgene [33]. We recovered 8–48 founder animals per each *Munc13-3* mutation (129 stocks in total), crossed them with a suitable Chr4-marker, and expanded the stocks.

All clonal fly strains, that is individual F1 progeny of each founder, proved fertile, demonstrating permanent correction of the *ovo*^{D1} allele in their genetic background. PCR-based genotyping confirmed successful integration of the individual missense mutations in *unc-13* in 34/129 (26%) *ovo*^{D1}-corrected lines cumulatively for all point mutations (see Table 2 for details). We crossed offspring from three independently recovered founder animals per human mutation over an embryonic lethal *unc-13*^{KO} null allele [29] in order to determine their genetic behavior (Fig. 2A). As each clonal population per individual *Munc13-3* mutation insertion was derived from founder animals, which received the same missense codon, we assumed that their offspring would show comparable quantitative outcome in this simple phenotypic assay. In contrast, transheterozygous *unc-13*^{X}/*unc-13*^{KO} offspring displayed pronounced differences in lethality. For example, when we analyzed *unc-13*$^{\#4}$/*unc-13*^{KO} transheterozygotes, two of the three analyzed lines showed Mendelian ratios that indicated no loss of UNC-13$^{\#4}$ function, while one displayed complete lethality (Fig. 2B). Similarly, also individual fly strains for mutations #3, #5, #6 and #7 exhibited differences in viability when the engineered *unc-13* mutation was uncovered by the *unc-13*^{KO} null allele. These results alerted us to a general problem regarding the targeting fidelity of our *ovo*^{D} co-selection approach.

In order to evaluate possible sequence errors introduced during the targeting and DSB repair procedures, we inspected the regions flanking the Cas9 cutting sites by Sanger sequencing. We found various nucleotide insertions or deletions at one or both sgRNA positions in almost each clonal *unc-13*^{X} strain leading to loss or gain of nucleotides, which resulted in additional missense or frame-shift mutations of the *unc-13* open-reading frame (ORF) (Fig. 2C). In order to test for additional undesired sequence modifications within the *unc-13* locus regions that are unrelated to the genomic sgRNA target positions, we sequenced the genomes of four clonal fly strains (Fig. 2D). This confirmed the presence of the sequence modifications at the Cas9 cleavage sites but did not reveal additional sequence errors that may account for the diverse genetic behavior of the individual *unc-13*^{X} alleles we constructed.

We concluded that the inadvertent genomic sequence errors at the sgRNA binding sites in targeted founders were locally confined due to the CRISPR/Cas9 targeting procedure. As the original sgRNA binding sites were reconstituted through the HDR of the engineered *unc-13* locus, we surmised that the indels were likely caused by repeated rounds of Cas9 cleavage of the already edited genomic DNA and its subsequent DSB repair. Ultimately, this likely resulted in erroneous deletion or incorporation of nucleotides rendering the targeting round futile.

Reduction of sgRNA binding site homology in HDR plasmids potently suppresses errors at Cas9 cleavage positions

In order to test this assumption and to recover incontestable *unc-13*^{X} alleles without inadvertent sequence abnormalities, we constructed a new set of HDR plasmids for cluster 1 mutations #2 and #3 (*pHDR-unc-13*$^{\#2\text{-}Fix}$, *pHDR-unc-13*$^{\#3\text{-}Fix}$). To prevent Cas9 processing of the successfully engineered locus DNA, we

Table 2: Overview of ovo^D-assisted gene targeting efficiency and precision of the *unc-13* locus without and with the use of modified sgRNA sites

Allele	With unmodified sgRNA sites in HDR plasmid, *n/N* (%)	With modified sgRNA sites in HDR plasmid, *n/N* (%)
unc-13$^{\#2}$		
No. of clonal F_1 offspring analyzed	21	20
With edited missense mutation	3/21 (14)	11/20 (55)
With correct unmodified/modified 5′-gRNA site sequence	1/3 (33)	11/11 (100)
With correct unmodified/modified 3′-gRNA site sequence	2/3 (67)	10/11 (91)
unc-13$^{\#3}$		
No. of clonal F_1 offspring analyzed	14	20
With edited missense mutation	3/14 (21)	10/20 (50)
With correct unmodified/modified 5′-gRNA site sequence	2/3 (67)	10/10 (100)
With correct unmodified/modified 3′-gRNA site sequence	0/3 (0)	10/10 (100)
unc-13$^{\#4}$		
No. of clonal F_1 offspring analyzed	14	Not applicable
With edited missense mutation	3/14 (21)	
With correct unmodified/modified 5′-gRNA site sequence	0/3 (0)	
With correct unmodified/modified 3′-gRNA site sequence	1/3 (33)	
unc-13$^{\#5}$		
No. of clonal F_1 offspring analyzed	24	Not applicable
With edited missense mutation	12/24 (50)	
With correct unmodified/modified 5′-gRNA site sequence	0/8 (0)	
With correct unmodified/modified 3′-gRNA site sequence	0/8 (0)	
unc-13$^{\#6}$		
No. of clonal F_1 offspring analyzed	8	Not applicable
With edited missense mutation	5/8 (63)	
With correct unmodified/modified 5′-gRNA site sequence	0/4 (0)	
With correct unmodified/modified 3′-gRNA site sequence	0/4 (0)	
unc-13$^{\#7}$		
No. of clonal F_1 offspring analyzed	48	Not applicable
With edited missense mutation	8/48 (17)	
With correct unmodified/modified 5′-gRNA site sequence	2/4 (50)	
With correct unmodified/modified 3′-gRNA site sequence	0/4 (0)	

Notes: For experimental sets using unmodified sgRNA sites, "correct" refers to their wild-type sequence, and for experiments using modified sgRNA sites, "correct" refers to the modified sequence.

modified both original sgRNA binding site sequences in the HDR plasmid by nucleotide exchanges yielding silent mutations, which would not cause amino acid changes in the gene products [9, 20, 21, 34]. Due to the positions of the PAM sequence of sgRNA binding sites 1 and 2 within the *unc-13* ORF, we could not simply inactivate the PAMs through point mutations of the two 3′-*GG* PAM-nucleobases without impacting amino acid coding. Instead, we exchanged 7 nt and 5 nt of the 23-bp spanning sgRNA binding sites 1 and 2, respectively, to reduce their homology and, consequently, affinity to the cognate sgRNA probes (Fig. 1E). We reasoned that this intervention would render the successfully edited *unc-13* locus refractory to subsequent rounds of Cas9 cleavage.

We then repeated ovo^D-assisted CRISPR/Cas9 editing for *unc-13*$^{\#2}$ and *unc-13*$^{\#3}$ mutations using the modified HDR plasmids. After recovery of transformants and the generation of stably balanced stocks, we determined the presence of the *Munc13-3* missense mutations and noted that 11/20 lines for *unc-13*$^{\#2}$ and 10/20 lines for *unc-13*$^{\#3}$ targeting (in total 53%) contained the edited codons (Table 2). This indicated that the high efficiency of the editing procedure under ovo^D co-selection did not suffer from the changes to the sgRNA bindings sites in the HDR plasmids.

When we inspected the Cas9 cleavage positions in genomic DNA of individually established clonal fly strains carrying the *unc-13* alleles by Sanger sequencing, we found that only 1 out of 42 investigated target sites showed undesired changes that deviated from the modified sgRNA binding site sequences (Table 2). This confirmed that the HDR plasmid sequence modifications effectively suppressed all events that caused inadvertent sequence changes in the edited locus, for example, by quelling repeated rounds of endonuclease cleavage followed by DSB repair, and allowed for the successful recovery of ovo^{D1} co-selected transformants.

Bi-directional integration of sgRNA masking mutations 5′ to Cas9 cleavage sites suggests multiple repair mechanisms including synthesis-dependent strand annealing-aided repair

In addition, we observed that the sgRNA binding site masking mutations encoded on the HDR plasmids, which are largely located 5′ of the DSB generated by Cas9 cleavage, were introduced into the genomic DNA of engineered fly stocks with high efficiency (*unc-13*$^{\#2mod}$: 5′-Cas9 cut: 11/11 lines; 3′-Cas9 cut: 10/11 lines; *unc-13*$^{\#3mod}$: 5′-Cas9 cut: 10/10 lines; 3′-Cas9 cut: 10/10 lines; Fig. 3A and B). Those mutations appear inaccessible for repair mechanisms that involve only DNA synthesis in 5′- to 3′-direction at the Cas9 cleavage points followed by ligation to restore duplex DNA. This result thus suggests that HDR during the employed CRISPR/Cas9 editing procedures utilized synthesis-dependent strand annealing (SDSA) as a principal repair mechanism (Fig. 3C) [35].

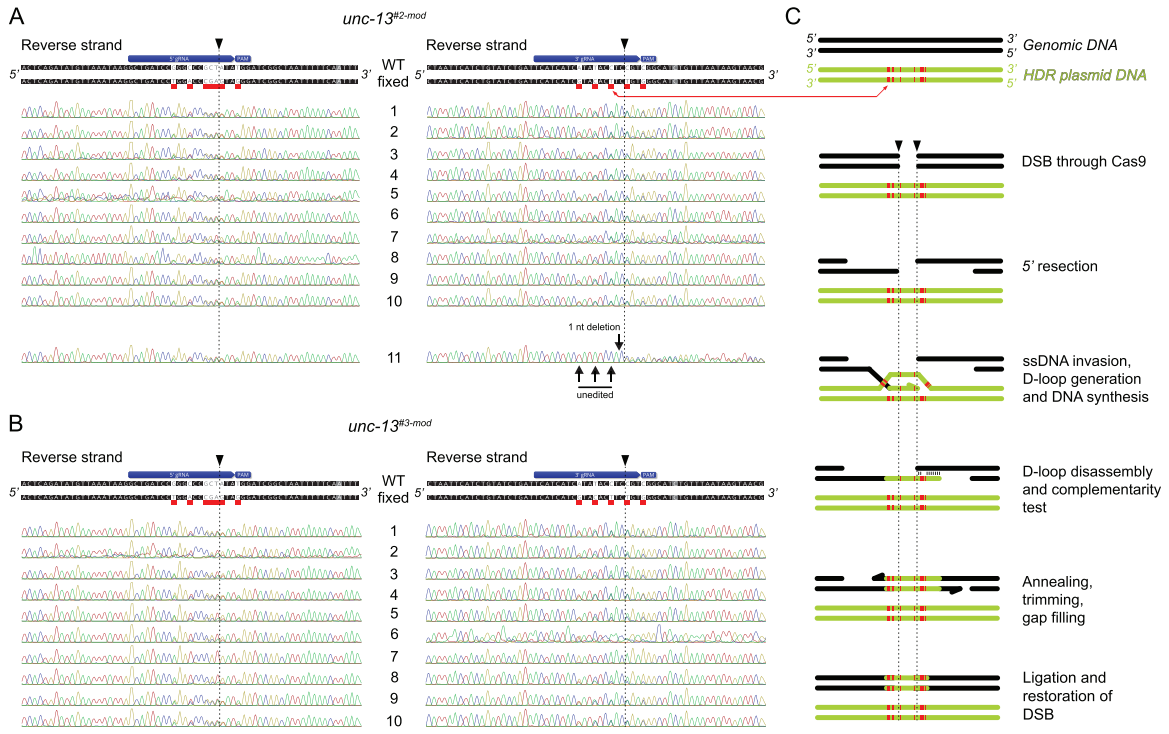

Figure 3: Sanger sequencing of *ovo*^{D}-assisted CRISPR/Cas9 shows introduction of modified sgRNA target/PAM sites in edited *unc-13*$^{\#2}$ and *unc-13*$^{\#3}$ mutants likely involving SDSA as a repair mechanism. (**A** and **B**) Sequence of wild-type (WT) and modified (fixed; red boxes underneath sequences) sgRNA and PAM sites are indicated above sequence chromatograms for individual stocks, in which mutations (A) *unc-13*$^{\#2}$ (11 lines) or (B) *unc-13*$^{\#3}$ (10 lines) were targeted (noted as *unc-13*$^{\#2\text{-}mod}$ and *unc-13*$^{\#3\text{-}mod}$). Note that sequenced animals contained a balancer chromosome and were thus mostly heterozygous hence double peaks are apparent at modified sgRNA/PAM positions in most lines. Only one Cas9 cleavage site contained an erroneous sequence (*unc-13*$^{\#2\text{-}mod}$, line 11, 3′-gRNA site). Reverse strand, in respect to direction of *unc-13* gene. (**C**) Principal steps of SDSA-dependent DSB repair that is involved in HDR during CRISPR/Cas9 engineering. Red blocks indicate masking point mutations in sgRNA binding and PAM sites in HDR plasmids. Note that through SDSA (only invasion by one strand shown here) also point mutations that are located 5′ of the Cas9 cleavage sites (dotted lines) can be incorporated in the modified genomic DNA. D-loop, displacement loop; ssDNA, single-stranded DNA. Schematic adapted from [35].

Mutagenesis of PAM sites in HDR plasmids improves targeting success under *ovo*^{D} co-selection

Finally, we tested the applicability of our modified targeting workflow with another independent *Drosophila* locus. We selected the human *β*-catenin 1 homolog *CTNNB1*, which is encoded by the *armadillo/arm* locus in the fly [36] (Fig. 4A) and which is not genetically linked to *unc-13*. Mutations of the *β-catenin 1* gene are notorious for their roles in a broad spectrum of human neoplasms such as tumors of the brain, the skin, or the intestine [37–39]. However, detailed analysis of the molecular effects caused by *CTNNB1* mutations is hampered by the lack of *in vivo* models that can aid in establishing causality in *β*-catenin structure–function relationships [40, 41].

We constructed and injected two sets of sgRNA and HDR plasmids to place four clinically relevant *CTNNB1* mutations (Table 1), some of which affect *β*-catenin phosphorylation [42, 43], in the *arm* locus through CRISPR/Cas9 editing under *ovo*^{D} co-selection (Fig. 4B). Similar to our initial *unc-13* strategy, the sgRNA binding site sequences in the HDR plasmids were left unchanged in the first *arm* transgenesis set so they remained homologous to the genomic sequence of the target *arm* locus. For the second set of injections, the PAMs of the 5′- and 3′-sgRNA binding site sequences in the HDR plasmids were disabled by one or two innocuous point mutations, respectively (Fig. 4C).

After injection of the first plasmid set, emerging founder females were recovered and balanced over an X-chromosomal balancer. Through PCR-based sequencing of the targeted *CTNNB1* mutations, we could not recover a single *ovo*^{D1}-rescued animal with a desired *arm* mutation (0/38) (for details, see Table 3). This suggested that similar problems as in the initial *unc-13* targeting attempt occurred also during the *arm* targeting procedure, for example, that unabated Cas9 activity of the engineered locus resulted in detrimental genome alterations, which ultimately precluded the development of founder animals. In contrast, after transgenesis using the modified HDR plasmids for two *arm* alleles, we established 32 clonal founder strains, of which 15 contained the inserted point mutation indicating an *ovo*^{D} co-selection efficiency of 47 %. None of those *arm* edited founders exhibited additional inadvertent sequence problems at or adjacent to the Cas9 cleavage sites as shown by PCR-based sequencing (Table 3).

We conclude that, as an alternative or in addition to reducing the homology of sgRNA binding sites, also mutagenesis of the PAM sequences in HDR plasmids for *Drosophila* genome editing can protect engineered loci from sequence errors at the sites of DSB repair.

Discussion

Here, we provide an optimized protocol for efficient and expedient use of *ovoD*-assisted CRISPR/Cas9-mediated mutagenesis. *ovo*^{D}-assisted CRISPR/Cas9-mediated genome engineering is an elegant strategy [17], which provides an effective approach to scarlessly engineer models of human disease-related point

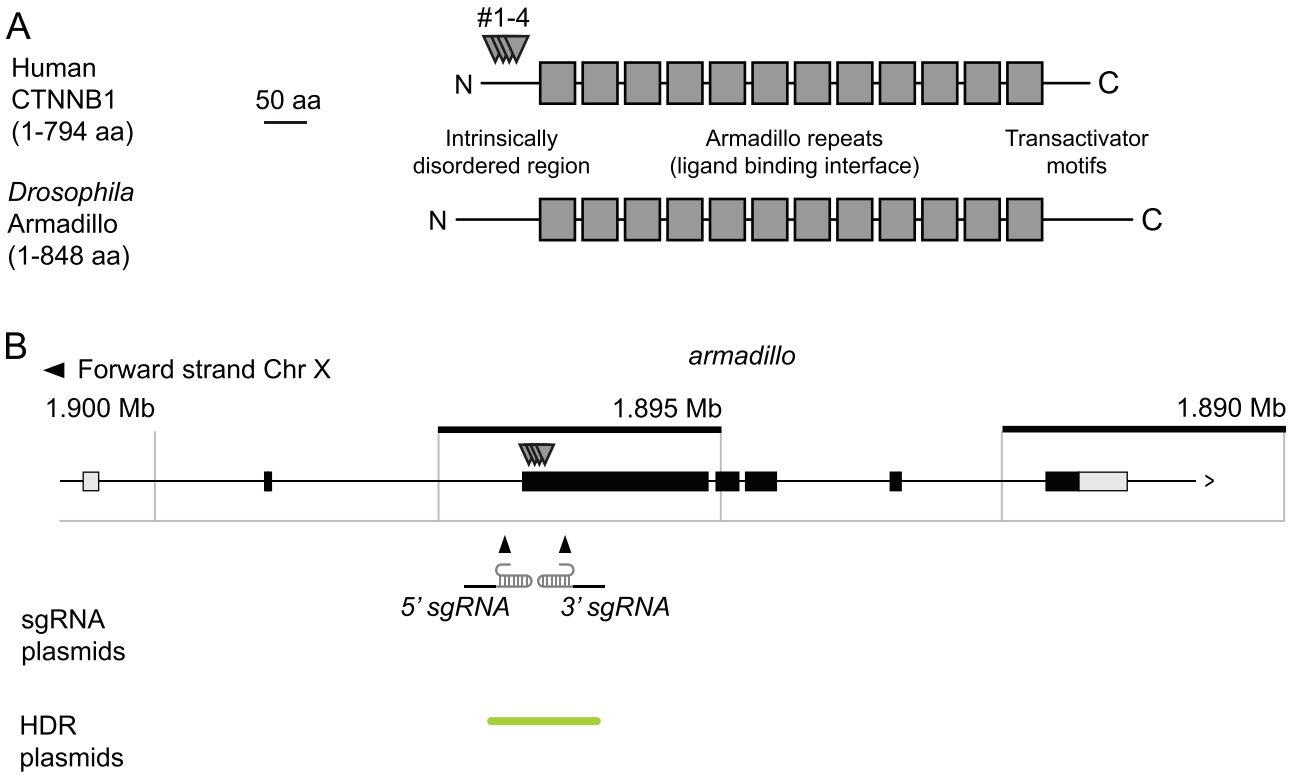

C

Site #	sgRNA sequence (5'-3') Distal	Proximal	PAM	Strand	OFF target #
5' sgRNA	AACATCTG	TCTACACATTCA	TGG	–	3 (2R, 2L,3L)
	tttATtTt	TCTACACATTCA	GGG		
	AACAatgG	TCTACgCATTCA	AGG		
	AcaATaTa	TgTACACATTCA	GGG		
HDR-fixed	**AACATCTG**	**TCTACACATTCA**	**Ttt**		
3' sgRNA	GTCACAAA	TGCTAAAGCACG	CGG	+	1 (2L)
	aTaAaAAg	TGCaAAAGCACG	CGG		
HDR-fixed	**GTCACAAA**	**TGCTAAAGCACG**	**CaG**		

Figure 4: *ovo*^{D}-assisted CRISPR/Cas9 editing of *arm* with masked PAM sites. (**A**) Schematic of the human CTNNB1 and the *Drosophila* Armadillo proteins. The ligand binding interface repeats are indicated by gray boxes. The human disease-associated mutations are indicated by downward triangles. (**B**) Schematic of the *Drosophila armadillo* gene structure. Black boxes indicate exons, light gray boxes show UTRs. The downward triangles mark the positions of the point mutations. (**C**) Nucleotide sequences of the sgRNAs used for Cas9 targeting of *armadillo*. Off-target binding sites are indicated in gray below the respective sgRNA binding site. Modified nucleotides for masking sgRNA binding sites in the HDR plasmid for improved *ovo*^{D}-assisted CRISPR/Cas9 targeting are marked by lowercase letters in red. Cas9 cleavage site is indicated by blue triangles. Strand direction relative to genomic *armadillo* sequence (+, forward strand; –, reverse strand).

mutations at large scale and study their consequences at the molecular, tissue, organ, and organism level. Our initial attempts to use this technique for direct exon editing without incorporation of a selection marker were, however, hampered by a low transgenesis efficiency (26% for *unc-13*, 0% for *arm* engineering) and by the incorporation of unwanted indels at Cas9 targeting sites due to intact sgRNA binding motifs in HDR donor plasmid constructs. This likely led to multiple rounds of Cas9 cleavage of the donor DNA and/or re-cleavage of the engineered locus and introduction of sequence errors by nonhomologous end joining rather than the desired HDR.

Earlier protocols proposed to prevent the potential re-cleavage of the exchanged DNA fragment by masking the sgRNA binding sites in the donor plasmid products [9, 20, 21, 34]. However, a quantitative assessment of such interventions to improve genomic engineering precision and efficiency in *Drosophila* – specifically in combination with *ovo*^{D} co-editing [17] – is lacking thus far. In the present study, we employed

Table 3: Overview of ovo^D-assisted gene targeting efficiency and precision of the *arm* locus without and with the use of modified PAM sites

Allele	With unmodified PAM site in HDR plasmid, *n*/*N* (%)	With modified PAM site in HDR plasmid, *n*/*N* (%)
arm^{WT}		
No. of clonal F_1 offspring analyzed	8	14
With edited missense mutation	0/8 (0)	3/14 (21)
With correct unmodified/modified 5′-PAM site sequence	–	3/3 (100)
With correct unmodified/modified 3′-PAM site sequence	–	3/3 (100)
$arm^{\#1}$		
No. of clonal F_1 offspring analyzed	13	NA
With edited missense mutation	0/13 (0)	
With correct unmodified/modified 5′-PAM site sequence	–	
With correct unmodified/modified 3′-PAM site sequence	–	
$arm^{\#2}$		
No. of clonal F_1 offspring analyzed	2	18
With edited missense mutation	0/2 (0)	12/18 (67)
With correct unmodified/modified 5′-PAM site sequence	–	12/12 (100)
With correct unmodified/modified 3′-PAM site sequence	–	12/12 (100)
$arm^{\#3}$		
No. of clonal F_1 offspring analyzed	8	NA
With edited missense mutation	0/8 (0)	
With correct unmodified/modified 5′-PAM site sequence	–	
With correct unmodified/modified 3′-PAM site sequence	–	
$arm^{\#4}$		
No. of clonal F_1 offspring analyzed	7	NA
With edited missense mutation	0/7 (0)	
With correct unmodified/modified 5′-PAM site sequence	–	
With correct unmodified/modified 3′-PAM site sequence	–	

Notes: For experimental sets using unmodified PAM sites, "correct" refers to their wild-type sequence, and for experiments using modified PAM sites, "correct" refers to the modified sequence.

mutagenesis masking of the PAM proximal region (see *unc-13* mutagenesis) or of the PAM site itself (see *arm* mutagenesis) and could demonstrate that the number of founder animals with correctly engineered loci increased to ∼50%.

For efficient and precise *unc-13* genome engineering, we inserted four to six non-PAM donor mutations to achieve potent suppression of sgRNA annealing to HDR plasmid DNA. Nonetheless, previous reports indicated that three mismatches suffice to prevent Cas9 cleavage [44]. The number of sgRNA binding site mutations may thus be reduced in future applications of our protocol, further simplifying the construction of suitable HDR plasmids for CRISPR/Cas9-mediated genome engineering (with and without ovo^D co-selection). Interestingly, the SDSA pathway is likely active in repairing DSBs during HDR gene editing events. Thus, it has been proposed to be the primary mechanism for integration of large insertions during genome editing with CRISPR/Cas9 [35, 45]. After annealing to the donor sequence, both 3′-ends are elongated and complementary strands are synthesized. These strands eventually hybridize to a double-strand accomplishing DSB repair. Elongation can exceed 4500 bp [35]. Our results are compatible with this assumption. As silent mutations located up- and downstream of the Cas9 cutting sites were incorporated into the target genome, a bidirectional repair mechanism such as SDSA is likely responsible for our observation. Genome sequencing showed no further alteration in the *unc-13* gene apart from single-nucleotide polymorphisms. Most deviations occurred in more than one clonal line and were unrelated to the mutation cluster.

CRISPR/Cas9 constitutes a valuable gene editing tool for *Drosophila* and other model species presenting a highly valuable basis for the investigation of human pathogenic gene sequence variants. Combined with a selection protocol based on ovo^D co-editing, rapid scarless editing is feasible even of exonic gene regions. Precision and efficiency of a HDR-mediated CRISPR/Cas9 targeting can, however, be profoundly hampered by unwanted re-cleavage and indel incorporation. Here we have re-assessed the technical means to circumnavigate these in the context of ovo^D co-editing by introducing silent sgRNA binding site mutations during HDR vector design problems [9, 20, 21 34], which efficiently suppress undesired Cas9 processing of the HDR plasmid before or of the engineered locus after transgenesis.

Supplementary data

Supplementary data are available at *Biology Methods and Protocols* online.

Data availability

Data are available in supplementary material. Plasmids, primers, genetic data and flies described in this article are also available upon request.

Acknowledgements

The authors acknowledge technical support from Andrea Böhme, Kerstin Heise and Maria Oppmann.

Author contributions

K.J.G. and A.M. performed the experiments, analyzed the data, and wrote the manuscript. P.B. performed the experiments. K.K., D.L.D., A.V., M.A.B., R.A.J., N.S. performed the

experiments and analyzed the data. M.H., J.R.L. and H.B. analyzed the data. D.L. and T.L. initiated the study, designed the experiments, analyzed the data, and wrote the manuscript.

Funding

This work was supported through grants of the Deutsche Forschungsgemeinschaft to T.L. (FOR2149 P01 [LA2861/4-2], P03 [LA2861/5-2], LA2861/7-1, CRC-TRR166/C03), to N.S. (FOR2149 P01 [SCHO1791/1-2]), and to T.L. and N.S. CRC 1423, 421152132, subprojects A06 and B06 and by the Else Kröner-Fresenius-Stiftung (2020_EKEA.42) to D.L.D. K.J.G. was funded by the "Promotionsförderung" program and D.L.D. is by the "Clinician Scientist Program" of the Medical Faculty of Leipzig University. We acknowledge support from Leipzig University for Open Access Publishing.

Conflict of interest statement. The authors declare no competing interests.

References

1. Cirulli ET, Goldstein DB. Uncovering the roles of rare variants in common disease through whole-genome sequencing. *Nat Rev Genet* 2010;**11**:415–25.
2. Gonzaga-Jauregui C, Lupski JR, Gibbs RA. Human genome sequencing in health and disease. *Annu Rev Med* 2012;**63**:35–61.
3. Claussnitzer M, Cho JH, Collins R *et al.* A brief history of human disease genetics. *Nature* 2020;**577**:179–89.
4. MacArthur DG, Manolio TA, Dimmock DP *et al.* Guidelines for investigating causality of sequence variants in human disease. *Nature* 2014;**508**:469–76.
5. Jinek M, East A, Cheng A *et al.* RNA-programmed genome editing in human cells. *eLife* 2013;**2**:e00471.
6. Cong L, Ran FA, Cox D *et al.* Multiplex genome engineering using CRISPR/Cas systems. *Science* 2013;**339**:819–23.
7. Mali P, Yang L, Esvelt KM *et al.* RNA-guided human genome engineering via Cas9. *Science* 2013;**339**:823–6.
8. Bassett AR, Tibbit C, Ponting CP *et al.* Highly efficient targeted mutagenesis of *Drosophila* with the CRISPR/Cas9 system. *Cell Rep* 2013;**4**:220–8.
9. Gratz SJ, Cummings AM, Nguyen JN *et al.* Genome engineering of *Drosophila* with the CRISPR RNA-guided Cas9 nuclease. *Genetics* 2013;**194**:1029–35.
10. Gratz SJ, Ukken FP, Rubinstein CD *et al.* Highly specific and efficient CRISPR/Cas9-catalyzed homology-directed repair in *Drosophila*. *Genetics* 2014;**196**:961–71.
11. Yu Z, Ren M, Wang Z *et al.* Highly efficient genome modifications mediated by CRISPR/Cas9 in *Drosophila*. *Genetics* 2013;**195**:289–91.
12. Port F, Chen H-M, Lee T *et al.* Optimized CRISPR/Cas tools for efficient germline and somatic genome engineering in *Drosophila*. *Proc Natl Acad Sci USA* 2014;**111**:E2967–76.
13. Fortini ME, Skupski MP, Boguski MS *et al.* A survey of human disease gene counterparts in the *Drosophila* genome. *J Cell Biol* 2000;**150**:23–30.
14. Reiter LT, Potocki L, Chien S *et al.* A systematic analysis of human disease-associated gene sequences in Drosophila melanogaster. *Genome Res* 2001;**11**:1114–25.
15. Chintapalli VR, Wang J, Dow JAT. Using FlyAtlas to identify better *Drosophila melanogaster* models of human disease. *Nat Genet* 2007;**39**:715–20.
16. Splinter K, Adams DR, Bacino CA *et al.*; Undiagnosed Diseases Network. Effect of genetic diagnosis on patients with previously undiagnosed disease. *N Engl J Med* 2018;**379**:2131–9.
17. Ewen-Campen B, Perrimon N. ovoD Co-selection: A method for enriching CRISPR/Cas9-edited alleles in *Drosophila*. *G3 (Bethesda)* 2018;**8**:2749–56.
18. DiCarlo JE, Norville JE, Mali P *et al.* Genome engineering in *Saccharomyces cerevisiae* using CRISPR-Cas systems. *Nucleic Acids Res* 2013;**41**:4336–43.
19. Horwitz AA, Walter JM, Schubert MG *et al.* Efficient multiplexed integration of synergistic alleles and metabolic pathways in yeasts via CRISPR-Cas. *Cell Syst* 2015;**1**:88–96.
20. Gratz SJ, Rubinstein CD, Harrison MM *et al.* CRISPR-Cas9 genome editing in *Drosophila*. *Curr Protoc Mol Biol* 2015;**111**:31.2.1–31.2.20.
21. Housden BE, Perrimon N. Design and generation of donor constructs for genome engineering in *Drosophila*. *Cold Spring Harb Protoc* 2016;**2016**:pdb.prot090787.
22. Levi T, Sloutskin A, Kalifa R *et al.* Efficient in vivo introduction of point mutations using ssODN and a Co-CRISPR approach. *Biol Proced Online* 2020;**22**:14.
23. Stokowy T, Eszlinger M, Świerniak M *et al.* Analysis options for high-throughput sequencing in miRNA expression profiling. *BMC Res Notes* 2014;**7**:144.
24. Li H, Durbin R. Fast and accurate short read alignment with Burrows–Wheeler transform. *Bioinformatics* 2009;**25**:1754–60.
25. Robinson JT, Thorvaldsdóttir H, Winckler W *et al.* Integrative genomics viewer. *Nat Biotechnol* 2011;**29**:24–6.
26. Cingolani P, Platts A, Wang LL *et al.* A program for annotating and predicting the effects of single nucleotide polymorphisms. *Fly (Austin)* 2012;**6**:80–92.
27. Talevich E, Shain AH, Botton T *et al.* CNVkit: Genome-wide copy number detection and visualization from targeted DNA sequencing. *PLoS Comput Biol* 2016;**12**:e1004873.
28. Augustin I, Rosenmund C, Südhof TC *et al.* Munc13-1 is essential for fusion competence of glutamatergic synaptic vesicles. *Nature* 1999;**400**:457–61.
29. Aravamudan B, Fergestad T, Davis WS *et al.* *Drosophila* Unc-13 is essential for synaptic transmission. *Nat Neurosci* 1999;**2**:965–71.
30. Richmond JE, Weimer RM, Jorgensen EM. An open form of syntaxin bypasses the requirement for UNC-13 in vesicle priming. *Nature* 2001;**412**:338–41.
31. Böhme MA, Beis C, Reddy-Alla S *et al.* Active zone scaffolds differentially accumulate Unc13 isoforms to tune Ca^{2+} channel–vesicle coupling. *Nat Neurosci* 2016;**19**:1311–20.
32. Betz A, Ashery U, Rickmann M *et al.* Munc13-1 is a presynaptic phorbol ester receptor that enhances neurotransmitter release. *Neuron* 1998;**21**:123–36.
33. Kondo S, Ueda R. Highly improved gene targeting by germline-specific Cas9 expression in Drosophila. *Genetics* 2013;**195**:715–21.
34. Port F, Bullock SL. Drosophila, methods and protocols. *Methods Mol Biol* 2016;**1478**:145–60.
35. Holsclaw JK, Sekelsky J. Annealing of complementary DNA sequences during double-strand break repair in *Drosophila* is mediated by the ortholog of SMARCAL1. *Genetics* 2017;**206**:467–80.
36. Peifer M, Wieschaus E. The segment polarity gene armadillo encodes a functionally modular protein that is the *Drosophila* homolog of human plakoglobin. *Cell* 1990;**63**:1167–78.
37. Miyaki M, Iijima T, Kimura J *et al.* Frequent mutation of beta-catenin and APC genes in primary colorectal tumors from

patients with hereditary nonpolyposis colorectal cancer. *Cancer Res* 1999;**59**:4506–9.
38. Logan CY, Nusse R. The WNT signaling pathway in development and disease. *Annu Rev Cell Dev Biol* 2004;**20**:781–810.
39. Zhang Y, Wang X. Targeting the Wnt/β-catenin signaling pathway in cancer. *J Hematol Oncol* 2020;**13**:165.
40. Kim S, Jeong S. Mutation hotspots in the β-catenin gene: lessons from the Human Cancer Genome Databases. *Mol Cell* 2019;**42**:8–16.
41. Arnold A, Tronser M, Sers C *et al.* The majority of β-catenin mutations in colorectal cancer is homozygous. *BMC Cancer* 2020;**20**:1038.
42. Liu C, Li Y, Semenov M *et al.* Control of β-catenin phosphorylation/degradation by a dual-kinase mechanism. *Cell* 2002; **108**:837–47.
43. Sadot E, Conacci-Sorrell M, Zhurinsky J *et al.* Regulation of S33/S37 phosphorylated beta-catenin in normal and transformed cells. *J Cell Sci* 2002;**115**:2771–80.
44. Ren X, Yang Z, Xu J *et al.* Enhanced specificity and efficiency of the CRISPR/Cas9 system with optimized sgRNA parameters in *Drosophila*. *Cell Rep* 2014;**9**:1151–62.
45. Nassif N, Penney J, Pal S *et al.* Efficient copying of nonhomologous sequences from ectopic sites via P-element-induced gap repair. *Mol Cell Biol* 1994;**14**:1613–25.